

Second Harmonic Generation in Polymer Photonic Integrated Circuits

Hauke Conradi , Almontaserbillah Hakmi , Moritz Kleinert , Lars Liebermeister, David de Felipe , Madeleine Weigel, Martin Kresse, Crispin Zawadzki, Björn Globisch , Norbert Keil , Ronald Freund, and Martin Schell

Abstract—Second harmonic generation is an efficient way to create coherent radiation at wavelengths that are not accessible with standard laser sources. In this work we demonstrate second harmonic generation from 1550 to 775 nm in a polymer photonic integrated circuit via the hybrid integration of a periodically poled lithium niobate crystal. The bulk crystal is inserted in an on-chip free-space section between two waveguide coupled GRIN lenses. Fiber to fiber conversion efficiencies were 0.03%/W for a continuous wave laser source and 100%/W for a femtosecond laser source. Furthermore, third and fourth harmonic light at 517 and 388 nm was observed.

Index Terms—Fourth harmonic generation, GRIN lenses, nonlinear optics, photonic integration, polymer waveguides, second harmonic generation, third harmonic generation.

I. INTRODUCTION

WITH the first demonstration of second harmonic generation (SHG) by Franken *et al.* [1], only one year after the development of an optical laser in 1961, nonlinear optics became an extensively studied field. Typical conversions include a pump wavelength in the infrared to create wavelengths ranging from the near infrared up to the green and blue optical spectrum [2], [3]. Most SHG setups use discrete optical elements and nonlinear crystals with a high second order nonlinearity $\chi^{(2)}$, for example lithium niobate (LN) or kalium titanyl phosphate (KTP), that are optically pumped at high intensities [3]–[5]. Besides a large nonlinear susceptibility, phase matching or quasi phase matching (QPM) between pump and second harmonic is

Manuscript received September 25, 2020; revised November 25, 2020; accepted December 3, 2020. Date of publication December 21, 2020; date of current version April 2, 2021. This work was supported by the European Commission through the Project ICT-3PEAT under Grant 780502 and Project ICT-UNIQUORN under Grant 820474. (Corresponding author: Hauke Conradi.)

Hauke Conradi, Almontaserbillah Hakmi, Moritz Kleinert, Lars Liebermeister, David de Felipe, Madeleine Weigel, Martin Kresse, Crispin Zawadzki, and Norbert Keil are with the Fraunhofer Heinrich Hertz Institute, 10587 Berlin, Germany (e-mail: hauke.conradi@hhi.fraunhofer.de; almontaserbillah.hakmi@hhi.fraunhofer.de; moritz.kleinert@hhi.fraunhofer.de; lars.liebermeister@hhi.fraunhofer.de; david.felipe@hhi.fraunhofer.de; madeleine.weigel@hhi.fraunhofer.de; martin.kresse@hhi.fraunhofer.de; crispin.zawadzki@hhi.fraunhofer.de; norbert.keil@hhi.fraunhofer.de).

Björn Globisch, Ronald Freund, and Martin Schell are with the Fraunhofer Fraunhofer Heinrich Hertz Institute, 10587 Berlin, Germany, and also with the Technical University of Berlin, 10623 Berlin, Germany (e-mail: bjoern.globisch@hhi.fraunhofer.de; ronald.freund@hhi.fraunhofer.de; martin.schell@hhi.fraunhofer.de).

Color versions of one or more figures in this article are available at <https://doi.org/10.1109/JLT.2020.3046371>.

Digital Object Identifier 10.1109/JLT.2020.3046371

required for efficient SHG, which can be achieved by periodic poling of the nonlinear crystal [1]–[5]. Integrated optics with single-mode optical waveguides provide an efficient way for SHG, as the strong optical confinement of the waveguide yields high power densities. Materials used for these nonlinear waveguides include LiNbO₃, AlGaAs, or nonlinear optical polymers, while quasi phase matching is achieved by periodic poling or modal phase matching [6]–[8]. Integration platforms based on silicon or silicon nitride utilize bulk induced stress and material interfaces to break the inversion symmetry, which is required to enable second order nonlinear processes [9].

In this work we demonstrate SHG in the polymer-based PolyBoard photonic integration platform, via hybrid integration of a periodically poled lithium niobate (ppLN) crystal into an on-chip collimated and focusing free-beam section. The photonic integrated circuit (PIC) features an on-chip free-space section, realized inbetween two graded index lenses (GRIN-lenses), which are coupled to polymer embedded waveguides via etched U-grooves. The advantage of this hybrid integration approach is the easy co-integration with already existing building blocks of the platform. These include thin film filter elements for spectral filtering and polarization handling, tunable DBR lasers, as well as isolators and circulators [11]–[13]. Here, we integrate a periodically poled lithium niobate (ppLN) bulk crystal with a length of 1 mm, designed for SHG with short laser pulses. To measure different aspects of the conversion efficiency, collimated beams and beams focused in the center of the crystal are evaluated in combination with continuous wave (cw) and femtosecond pulsed laser excitation.

II. OPERATION PRINCIPLE

The ppLN crystal is integrated with the PIC by inserting it into an on-chip collimated free-space section as depicted in Fig. 1.

To compensate for the beam divergence at the single-mode waveguide facet a first GRIN lens is used to create a collimated or focused Gaussian beam. A second GRIN lens after the free-space section couples the light back into the waveguide. This approach creates a section that enables the integration of bulk optical elements such as nonlinear crystals between the two GRIN lenses. By variation of the GRIN lens length, the optical beam inside the free-space section can be tailored, enabling the creation of a collimated or focused beam inside the crystal to enhance nonlinear conversion efficiencies.

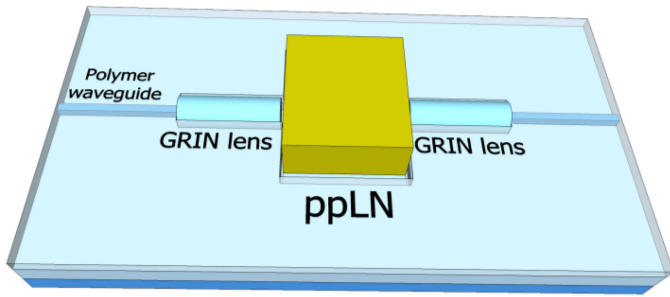


Fig. 1. Schematic layout of the proposed design for the ppLN integration with two GRIN lenses coupled to polymer waveguides to create an on-chip free-space section.

III. SIMULATION

The GRIN lenses used for the coupling process have a numerical aperture (NA) of 0.14 with a nearly parabolic refractive index profile inside the core. The diameter of the core is $100\ \mu\text{m}$ while the outer diameter matches a standard single mode fiber ($125\ \mu\text{m}$). By controlling the length of the GRIN lenses it is possible to tailor the beam propagation in the bulk ppLN and minimize coupling losses from the polymer waveguides to the free-space section and back into the polymer waveguide. In order to determine the optimal GRIN lens length for a given crystal length, simulations were carried out using the paraxial Gaussian beam approximation and the physical optics propagation analyzer from Zemax. For the simulations, a Gaussian mode with a $1/e^2$ mode field diameter (MFD) of $9.6\ \mu\text{m}$ was assumed for the single-mode polymer waveguides at $1550\ \text{nm}$. It is noted that the polymer waveguides are designed for wavelengths of $1550\ \text{nm}$, resulting in multimode behavior for the SH at $775\ \text{nm}$. However, it is possible to design waveguides that are single mode at both $775\ \text{nm}$ and $1550\ \text{nm}$, with highly confined modes at $775\ \text{nm}$ and weakly guided modes at $1550\ \text{nm}$, which will be done in a future iteration. The simulation model comprises the coupling from the input waveguide via the first GRIN lens into the free-space section with the ppLN crystal and via the second GRIN lens finally back into the output waveguide. Fig. 2 depicts the color-coded coupling efficiency as function of GRIN lens (y-axis) and crystal length between the two GRIN lenses (x-axis). For a given crystal length below $2\ \text{mm}$, four different solutions for optimal coupling can be found that converge into two solutions for larger crystal lengths. At a length of $0\ \text{mm}$ these correspond to the pitches 0.25 , 0.5 , 0.75 and 1 of the GRIN lenses, where a pitch of 1 is defined as a whole sinusoidal ray trace inside the GRIN lens [14]. The simulation shows, that crystal lengths of up to $7\ \text{mm}$ can be realized with coupling losses below $1\ \text{dB}$ at $1550\ \text{nm}$. Larger free-space lengths are still possible, but result in increasingly higher coupling losses due to the beam divergence and an increasing phase mismatch at the interface between the second GRIN lens and the polymer waveguide. The second harmonic created inside the crystal shares the same focal point as the pump wavelength, with a factor of $1/\sqrt{2}$ smaller MFD and the same Rayleigh length as the pump [15]. In combination with the negligible chromatic aberration of the optical system, this results in equally good coupling efficiencies from the second GRIN lens back into the polymer waveguide for the second harmonic.

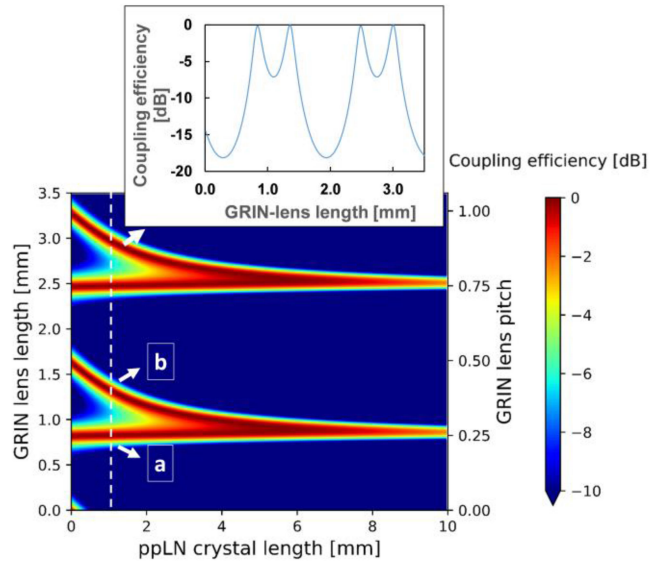


Fig. 2. Simulated coupling loss at a wavelength of $1550\ \text{nm}$ depending on the GRIN lens length and the length of the ppLN crystal in between the lenses. The dashed white line and the subplot correspond to a fixed crystal length of $1\ \text{mm}$ with highlighted optimal coupling GRIN lens lengths of $830\ \mu\text{m}$ (a) and $1330\ \mu\text{m}$ (b) that are depicted as radial Gaussian intensity distributions in Fig. 3.

The ppLN crystal, integrated into the free-space section, has a length of $1\ \text{mm}$. For a free-space section of $1\ \text{mm}$ and pitch < 0.5 , two solutions for minimal coupling loss with $l_{\text{GRIN}1} = 840\ \mu\text{m}$ (Fig. 3(a)) and $l_{\text{GRIN}2} = 1330\ \mu\text{m}$ (Fig. 3(b)) were found. The first one, $l_{\text{GRIN}1}$, corresponds to a GRIN lens pitch of ~ 0.25 . This GRIN lens length creates a collimated beam inside the free-space section with minimal beam divergence and a beam diameter of $80\ \mu\text{m}$. The second solution with a pitch of ~ 0.40 creates a focused Gaussian beam with a beam waist of $6\ \mu\text{m}$ in the center of the crystal. Both solutions are depicted as cross-sectional intensity distributions in Fig. 3. In general, GRIN lenses with a pitch of 0.25 are more versatile in their application, since they cover a broader range of free-space section lengths (Fig. 2), but in order to improve the conversion efficiency GRIN lenses with a pitch of 0.40 should yield a better result due to the focusing spot inside the crystal. The given GRIN lens and crystal length result in ratio of 2.5 between crystal length and confocal parameter, close to the Boyd-Kleinman condition of 2.83 for optimal focusing inside a crystal [15].

In order to determine the coupling tolerances, a vertical offset between the single-mode polymer waveguides and the GRIN lenses and a relative tilt of the input GRIN lenses were simulated. The results are shown in Fig. 4. An offset of $1\ \mu\text{m}$ or 1° correspond to coupling losses of $0.5\ \text{dB}$ and $5.8\ \text{dB}$ respectively. In general, offset values smaller than $\pm 1\ \mu\text{m}$, are well within the fabrication tolerances of the U-grooves used for the insertion of the GRIN lenses. The fabrication tolerances also ensure a tilt of $< 0.1^\circ$, since the lower contact area of the U-grooves can be used to align the GRIN lenses properly.

IV. FABRICATION

The ppLN crystal is placed into a PIC fabricated in the polymer-based hybrid photonic integration platform PolyBoard, which is based on a network of single mode waveguides

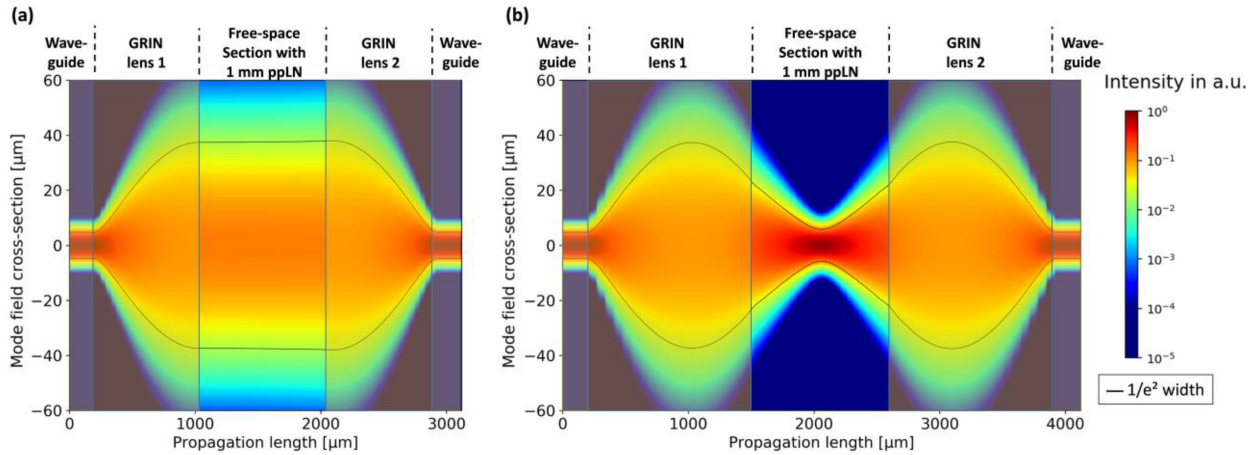


Fig. 3. Radial intensity distribution for a free-space length of 1 mm with a ppLN crystal inserted and a GRIN lens length of $840 \mu\text{m}$ (a) and $1330 \mu\text{m}$ (b) at 1550 nm wavelength, corresponding to the parameter combinations highlighted as [a] and [b] in Fig. 2.

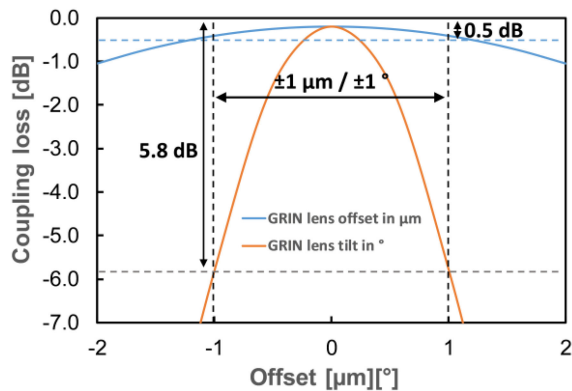


Fig. 4. Coupling tolerances of a free-space section for a vertical offset (blue line) and a tilt (grey line) for GRIN lens lengths of 0.84 mm and a free-space section of 1.0 mm .

embedded into a polymer cladding material. Both, cladding and core material are spin coated as a liquid resin onto a silicon substrate wafer, UV cured and hard baked. Structuring of the waveguides and other optical functionalities is done by photo lithography and reactive ion etching (RIE).

A refractive index difference of $\Delta n = 0.005$ between cladding and core with a core size of $7.3 \mu\text{m}$ by $7.3 \mu\text{m}$ was chosen. This results in a MFD of $9.6 \mu\text{m}$.

The deep U-grooves used to hold the GRIN lenses are fabricated via inductively coupled plasma-RIE. For efficient GRIN lens coupling this etching process requires a vertical precision of $\pm 1 \mu\text{m}$ across the $4''$ wafer to stay well inside the tolerated offsets simulated in Fig. 4. Lateral offsets are negligible, as they are given by the resolution of the lithographic fabrication processes. Fig. 5 depicts the cross-section of such a U-groove, which can be used for passive coupling of either single mode fibers or GRIN lenses.

The GRIN lenses are fabricated from a graded index fiber with a NA of 0.14 , and a core/cladding diameter of $100 \mu\text{m}/125 \mu\text{m}$. In a lapping and polishing process, two batches of lenses are shortened to the target lengths of $840 \mu\text{m}$ and $1330 \mu\text{m}$, according to the results of Section III.

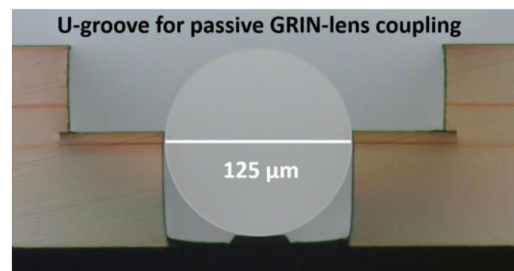


Fig. 5. Cross-section of a U-groove for passive GRIN lens coupling. The grey circle highlights the position of the GRIN lens.

The fabricated device consists of an input and output waveguide, coupled to two GRIN lenses inserted into U-grooves. Due to the precisely etched U-grooves, the GRIN lenses are aligned passively to the waveguides. A free-space section of 1.0 mm in between allows for the insertion of a commercially available anti reflection coated ppLN crystal for SHG from 1550 nm to 775 nm , with a poling period of $19.1 \mu\text{m}$ fabricated by Covision Ltd. The effective nonlinear coefficient of the crystal is $d_{\text{eff}} = 14 \text{ pm/V}$, with $d_{33} = 25 \text{ pm/V}$ being the highest nonlinear coefficient [16]. Thus, both pump and second harmonic are TM polarized, and SHG occurs via type-0 phase matching. Phase matching for 1550 nm is achieved at a temperature of 100°C , with a spectral acceptance bandwidth of 12 nm .

The crystal is manually placed into the free-space section. Its vertical position is automatically aligned through contact with the bottom of the free-space section defined by RIE. Horizontally, the crystal is actively aligned with a micro manipulator, monitoring and minimizing transmission loss at 1550 nm . (Automizing placement and alignment using a FICONTEC CL1500 machine is under development). Both, the GRIN lenses and the ppLN crystal are fixed with UV index matching glue after the alignment process.

In order to investigate the conversion efficiency, two types of devices were fabricated, matching the different lengths of fabricated GRIN lenses. A micrograph of both fabricated devices is shown in Fig. 6.

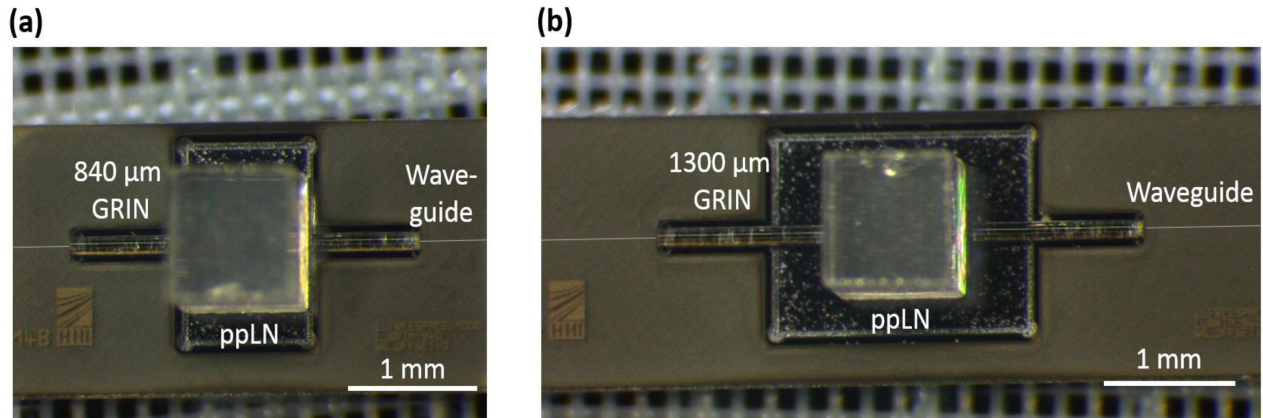


Fig. 6. Fabricated devices with collimating GRIN lenses (a) and focusing lenses (b) with highlighted polymer waveguides before applying index matching glue to fix the crystal and lenses.

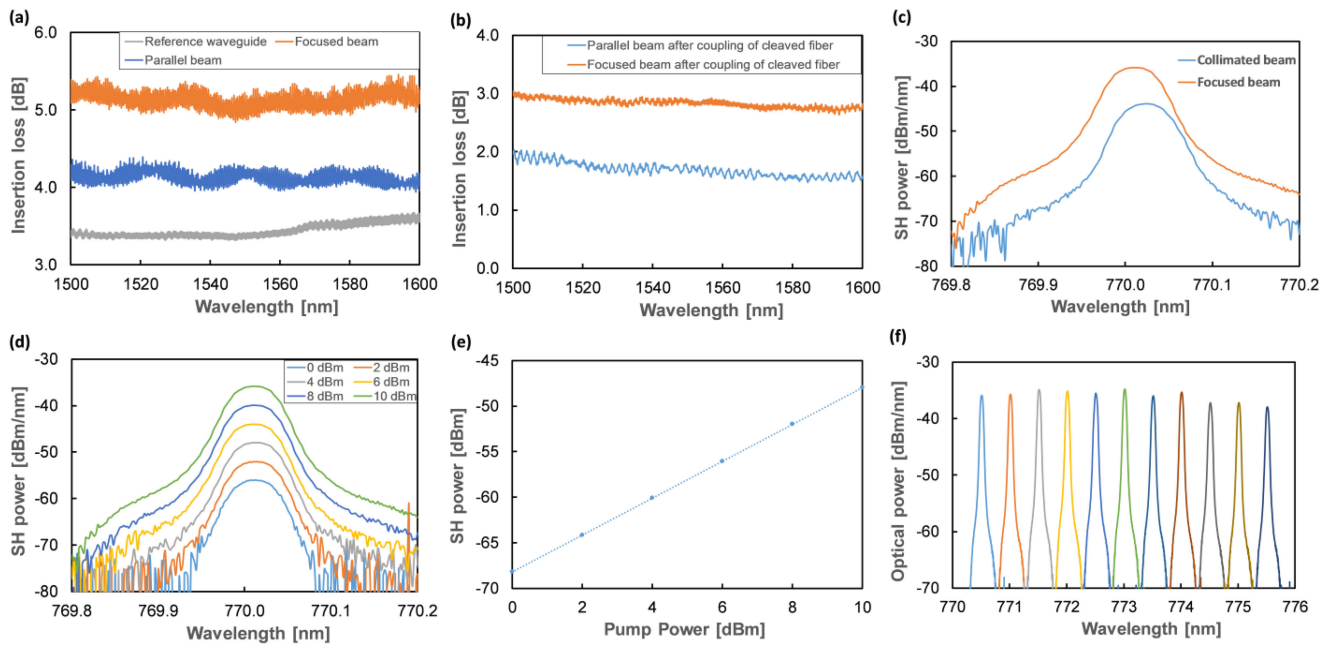


Fig. 7. (a) Insertion loss of the fabricated devices with $830 \mu\text{m}$ GRIN lenses for a collimated beam (blue curve), $1300 \mu\text{m}$ GRIN lenses for a focused beam (orange) and an adjacent straight reference waveguide (grey), measured with lensed fibers. (b) Insertion loss for both devices after fixation of input and output cleaved fibers. (c) SH spectrum of collimating and focusing GRIN lenses. (d) influence of the pump power onto the output spectrum of the SH. (e) Plotting the SH power against the pump power in a double logarithmic scale yields in a linear relationship with a slope of 2.02, which is in good agreement with the theoretical quadratic prediction. (f) Tuning of the SH for a fixed temperature of 40°C .

V. RESULTS

The fully assembled chips with inserted ppLN crystals are characterized by measuring the insertion loss between 1500 nm and 1600 nm. Fig. 7(a) shows the total insertion loss for the collimated and focused integration together with the transmission through one adjacent straight reference waveguide. The measurements include the fiber-chip-fiber coupling loss of 1.5 dB per facet measured with $6 \mu\text{m}$ spot size lensed fibers and waveguide propagation loss (0.7 dB/cm) at 1550 nm. For the collimating GRIN lenses, an excess loss of $<0.7 \text{ dB}$ with respect to a straight reference waveguide was calculated by subtracting the reference waveguide loss from the device loss. For the focussing lenses, an excess loss of $<1.8 \text{ dB}$ was measured. After this

pre-characterization with lensed fibers, used for the alignment and fixation of the GRIN lenses and the ppLN, two SMF-28 fibers with a MFD of $10.4 \mu\text{m}$ at 1550 nm were actively aligned to the input and output waveguide and fixed with index matching glue. This reduces the coupling loss to 0.5 dB per coupling interface (Fig. 7(b)), while simultaneously reducing the spectral oscillations from back reflections at the waveguide facets.

To determine the conversion efficiency of the collimated and the focused device, both are characterized with a cw laser source at a wavelength of 1540 nm and a pump power of 10 dBm. The temperature of the chip is fixed at 40°C . It is noted that both, the output waveguide and the output SMF, are multimode at 775 nm since they are designed and specified for a wavelength of 1550 nm, but the additional loss at 775 nm is negligible for

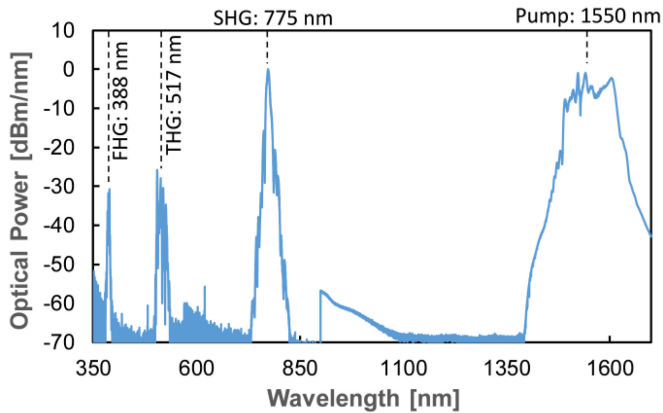


Fig. 8. Optical spectrum for focusing lenses with the pump of the femtosecond laser around 1550 nm, the SHG at 775 nm and weak peaks of the third harmonic (THG) at 517 nm and the fourth harmonic (FHG) at 388 nm.

short fiber lengths. The output power spectrum of the second harmonic is measured with an optical spectrum analyser in order to determine the conversion efficiency. The 3 dB bandwidth output power of the second harmonic is calculated directly from the spectrum. Fig. 7(c) shows the spectra for both devices. For the collimated beam an output power of -57 dBm was achieved. With the focused beam configuration, an 8 dB improvement could be achieved resulting in -49 dBm. These output powers correspond to conversion efficiencies of $0.005\%/W$ and $0.03\%/W$ for the collimated and the focusing lenses respectively.

Plotting different second harmonic powers against the pump power in a double logarithmic scale yields a slope of 2.02 ± 0.02 between both values, which is in good accordance with the theoretical quadratic relationship between pump power and second harmonic (Fig. 7(d) and (e)) [15]. For a fixed temperature of 40°C the tuneability of the second harmonic is determined by varying the pump wavelength from 1540 nm to 1550 nm (Fig. 7(f)). At longer wavelengths, a decrease in the output power is observed due to higher phase mismatch between pump wavelength and its second harmonic. Because of the short crystal length of 1 mm, resulting in a high temperature acceptance bandwidth, there is only a small reduction in output power. However, keeping a constant output power for increasing wavelengths can be realized with a higher crystal temperature.

A significant increase of the conversion efficiency is expected for pumping with a femtosecond pulsed laser. For the following experiment a femtosecond laser with an average power of 19 dBm, 100 MHz repetition rate, and a pulse duration of ~ 120 fs was used. This results in pump peak powers of 68 dBm. The SHG output power increases to 8.2 dBm, which is an improvement of 54 dB compared to the cw pump mentioned earlier. The optical spectrum of the pulsed SHG is depicted in Fig. 8. The measurement was done at room temperature using an assembled chip with focused beam configuration.

As result of the high peak intensities of the pump, not only the second harmonic at 775 nm but also weak intensities of the third harmonic at 517 nm and the fourth harmonic at 388 nm were generated. Calculating the output power from the peak

intensities in Fig. 8 with respect to the input power results in 8.2 dBm output power for the SHG from 1550 nm to 775 nm, -20.6 dBm for the third harmonic and -28.0 dBm for the fourth harmonic. These values correspond to a conversion efficiency of -11 dB ($\sim 8\%$) for SHG and -39 dB and -44 dB for the third and fourth harmonic generation respectively. The optical power of all higher harmonics was calculated within a 10 dB peak bandwidth. Please note that no deterioration of the polymer material was observed, even though pump peak powers of 6.7 kW were transferred into the polymer waveguides. However after ~ 1 hour of testing, the UV curing glue used to fix the input fiber started to deteriorate, making it not suitable for these high optical powers.

VI. DISCUSSION

The overall conversion efficiency for a cw laser source in this work is limited with values of $0.005\%/W$ and $0.03\%/W$ but in good agreement with the theoretical work in [15], when additional on-chip and fiber chip coupling losses are taken into account. The reason for the higher loss of the focused free-space section (Fig. 7(a)) is a deviation of the fabricated $1300 \mu\text{m}$ long GRIN lenses from the targeted $1330 \mu\text{m}$ length, corresponding to the optimal value calculated in Section III. Using focusing lenses instead of a collimated free-space beam increases the efficiency by 8 dB (factor of ~ 6). Since the output power of the second harmonic scales quadratically with the crystal length and the pump power, the best way to improve the cw conversion efficiency is via the length of the crystal. According to Fig. 2, crystal lengths of up to 5 mm should be possible without a significant increase in loss. However, the focusing quality of the GRIN lenses for longer free-space sections is limited, resulting in an increasing deviation from the Boyd-Kleinman condition for optimal focusing. Taking this into account the calculated conversion efficiency for a 5 mm long crystal would be $\sim 0.7\%/W$ for a single pass experiment, without consideration of any on-chip and fiber coupling loss. Since the beam divergence of a Gaussian beam scales inversely with the beam waist, doubling the GRIN lens diameter (and thus the beam waist) would also double the possible length of crystals inside the free-space section. The most promising way to increase the conversion efficiency is the development of a resonant or double resonant cavity design. Even for moderate pump powers and small crystal lengths high conversion efficiencies have been demonstrated with this approach in bulk optics [17] and in microring resonators demonstrated in thin-film lithium niobate and silicon nitride platforms [18]–[20]. Development of a stable resonant cavity with the on-chip integrated GRIN lenses is possible by applying high reflective coatings to the waveguide oriented facets of the GRIN lenses or waveguide inscribed Bragg-gratings at the input and output waveguides and is currently under investigation. Due to their strong phase sensitivity, hitherto free beam resonant and double resonant schemes are expected to benefit most from the photonic integration of nonlinear crystals shown in this paper.

For the pulsed laser source, a SHG output power of 6.6 mW with a total SHG conversion efficiency of 8% ($100\%/W$) with

respect to the 80 mW input pump power was achieved. In this work the conversion efficiency is limited by the 12 nm bandwidth of the 1 mm long ppLN crystal, compared to the much larger bandwidth of the femtosecond laser (~ 120 nm for 10 dB bandwidth). Thus, only a fraction of the pump power within the 12 nm bandwidth of the crystal contributes to the SHG. Since the SHG bandwidth scales inversely with crystal length, the integration of a shorter crystal would be beneficial for the pulsed laser source in contrast to the cw use case described above. A shorter crystal would also reduce the gap between recently reported values of 50% conversion efficiency in nanophotonic ppLN waveguides [21] and this work. The advantage of the nonlinear waveguides described in [18]–[21] is the required low pump power for SHG and small footprint compared to ppLN bulk crystals. In principle it should also be possible to integrate ppLN waveguides into dedicated and precisely etched U-grooves, with butt coupling of the ppLN to polymer waveguide. This approach could combine the high conversion efficiencies of these waveguides with available building blocks of the PolyBoard, like tunable lasers or thin film filters for efficient spectral filtering.

The observed third harmonic is created by sum frequency generation of the SH and the pump, enabled by third order quasi phase matching. Frequency doubling of the second harmonic also creates the fourth harmonic at 388 nm. Even though only small intensities of the higher harmonics were measured, with our approach it would be possible to build PICs based on the cascaded integration of crystals that are specifically designed for third and fourth harmonic generation as already demonstrated in bulk optics [22].

VII. CONCLUSION

We proposed, designed and fabricated a polymer-based integrated SHG source utilizing the hybrid integration of a ppLN bulk crystal via GRIN lenses. SHG sources with collimated and focused free-space sections were characterized with a cw laser and a femtosecond pulsed laser source. The fabricated devices exhibit on-chip loss of 0.7 dB and 1.8 dB at 1550 nm, demonstrating the low loss and small footprint integration of nonlinear crystals into polymer PICs. Maximum conversion efficiencies of 100%/W (8% total conversion efficiency) for a 80 mW pulsed laser source and 0.03%/W for cw operation were achieved. While second harmonic generation with a femtosecond laser is already efficient due to the high pump peak power, the CW conversion efficiency could be further improved by increasing the crystal length and the development of a resonant cavity design in the on-chip free-space section. Together with other building blocks available on the PolyBoard such as thin film filter elements for spectral and polarization filtering, tunable DBR lasers and the large transparency range of polymers down into the visible light spectrum, the hybrid integration of nonlinear crystals into PICs described in this work opens up a large field of applications not only for wavelength tailored higher harmonic generation, but also for other nonlinear processes like SPDC which is widely used for the creation of single photons and entangled photons.

REFERENCES

- [1] P. A. Franken *et al.*, "Generation of optical harmonics," *Phys. Rev. Lett.*, vol. 7, no. 4, pp. 118–119, 1961.
- [2] E. J. Lim *et al.*, "Second-harmonic generation of green light in periodically poled planar lithium niobate waveguide," *Electron. Lett.*, vol. 25, no. 3, pp. 174–175, 1989.
- [3] M. Yamanda *et al.*, "First order quasi-phase matched linbo3 waveguide periodically poled by applying an external field for efficient blue second-harmonic generation," *Appl. Phys. Lett.*, vol. 62, no. 5, pp. 435–436, 1993.
- [4] G. D. Miller *et al.*, "42%-efficient single-pass cw second-harmonic generation in periodically poled lithium niobate," *Opt. Lett.*, vol. 22, no. 24, pp. 1834–1836, 1997.
- [5] J. D. Bierlein and H. Vanherzeele, "Potassium titanyl phosphate: Properties and new applications," *J. Opt. Soc. Amer.*, vol. 6, no. 4, pp. 622–633, 1989.
- [6] B. Jaskorzynska *et al.*, "Periodic structures for phase-matching in second harmonic generation in titanium lithium niobate wave guides," in *Proc. SPIE 0651, Integr. Opt. Circuit Eng. III*, 1986.
- [7] K. Moutzouris, "Second-harmonic generation through optimized modal phase matching in semiconductor waveguides," *Appl. Phys. Lett.*, vol. 83, no. 4, pp. 620–622, 2003.
- [8] G. Khanarian *et al.*, "Phase-matched second harmonic generation in a polymer waveguide," *Appl. Phys. Lett.*, vol. 57, no. 10, pp. 977–979, 1990.
- [9] M. Cazzanelli *et al.*, "Second-harmonic generation in silicon waveguides strained by silicon nitride," *Nat. Mater.*, vol. 11, pp. 148–154, 2012.
- [10] M. Happach *et al.*, "On-chip free beam optics on a polymer-based photonic integration platform," *Opt. Express*, vol. 25, no. 22, pp. 27665–27670, 2017.
- [11] H. Conradi *et al.*, "High isolation optical isolator: A new building block for polyboard photonic integrated circuits," in *Proc. Eur. Conf. Opt. Commun.*, 2018, pp. 1–3.
- [12] H. Conradi *et al.*, "Hybrid integration of a polarization independent optical circulator," in *Proc. SPIE*, 2020, Art. no. 112830J.
- [13] M. Kleinert *et al.*, "Photonic integrated devices and functions on hybrid polymer platform," in *Proc. SPIE*, 2017, Art. no. 100981A.
- [14] R. Gilsdorf and J. Palais, "Single-mode fiber coupling efficiency with graded-index rod lenses," *Appl. Opt.*, vol. 33, no. 16, pp. 3440–3445, 1994.
- [15] G. Boyd and D. Kleinman, "Second-harmonic generation of light by focused laser beams," *Phys. Rev.*, vol. 125, no. 1, pp. 338–379, 1966.
- [16] W. P. Risk *et al.*, *Compact Blue-Green Lasers*. Cambridge, U.K.: Cambridge Univ. Press, 2003.
- [17] W. J. Kozlovsky, C. D. Nabors, and R. L. Byer, "Efficient second harmonic generation of a diode-laser-pumped CW Nd:YAG laser using monolithic mgo:Linbo3 external resonant cavities," *IEEE J. Quantum Electron.*, vol. 24, no. 6, pp. 913–919, Jun. 1988.
- [18] J. Lu *et al.*, "Periodically poled thin-film lithium niobate microring resonators with a second-harmonic generation efficiency of 250,000%/W," *Optica*, vol. 6, no. 12, pp. 1455–1460, 2019.
- [19] X. Guo *et al.*, "Second-harmonic generation in aluminum nitride microrings with 2500%/W conversion efficiency," *Optica*, vol. 3, no. 10, pp. 1126–1131, 2016.
- [20] X. Lu *et al.*, "Efficient photoinduced second-harmonic generation in silicon nitride photonics," *Nature Photon.*, 2020, doi: [10.1038/s41566-020-00708-4](https://doi.org/10.1038/s41566-020-00708-4).
- [21] M. Jankowski *et al.*, "Ultrabroadband nonlinear optics in nanophotonic periodically poled lithium niobate waveguides," *Optica*, vol. 7, no. 1, pp. 40–46, 2020.
- [22] K. Moutzouris *et al.*, "Highly efficient second, third and fourth harmonic generation from a two-branch femtosecond erbium fiber source," *Opt. Express*, vol. 14, no. 5, pp. 1905–1912, 2006.

Hauke Conradi received the master's degree in physics from the Westfälische Wilhelms-Universität Münster, Münster, Germany. He is currently working toward the Ph.D. degree with the Hybrid PICs Group, Fraunhofer Heinrich Hertz Institute (HHI), Berlin, Germany, working on the hybrid photonic integration of nonlinear and nonreciprocal elements in polymer photonic integrated circuits. In 2017, he joined Fraunhofer HHI as a Research Associate.

Almontaserbillah Hakmi received the bachelor degree in electronics and telecommunications engineering from the University of Kalamoon, Deir Atiyah, Syria. Since 2017, he has been working toward the master's degree in electrical engineering with the Technical University of Berlin, Berlin, Germany, with a minor in communication systems. Since 2018, alongside his master studies, he has been a Student Research Assistant with Fraunhofer Heinrich Hertz Institute, Berlin, Germany, and the work of his paper is the topic of his master's thesis.

Moritz Kleinert received the master's degree from the Technical University of Berlin, Berlin, Germany, where he received the Ph.D. degree for his work on the hybrid photonic integration of graphene-based optoelectronic devices in 2018. In 2013, he joined Fraunhofer Heinrich Hertz Institute (HHI), Berlin. He is currently the Project Manager with the Hybrid PICs Group. He has authored or coauthored more than 40 papers in international journals and conference contributions.

Lars Liebermeister received the Ph.D. degree in quantum- and nanophotonics from Ludwig-Maximilians-Universität Munich, Munich, Germany, in 2016. Since 2017, he has been with the Terahertz Sensors and Systems Group, Fraunhofer Heinrich Hertz Institute, Berlin, Germany, as a Project Leader and Deputy Group Leader. His current research interests include integrated terahertz photonics, optoelectronic terahertz systems, and terahertz quantum optics.

David de Felipe received the Telecommunications Engineering degree from the Universitat Politècnica de València, València, Spain, in 2010 and the Ph.D. degree from the Technical University of Berlin, Berlin, Germany, for his work on hybrid polymer-based integrated tunable lasers. In 2011, he joined the Fraunhofer Heinrich Hertz Institute, Berlin, Germany, as a Research Associate. He has authored or coauthored more than 50 scientific publications and conference papers. He is currently working as a Project Manager for several European projects. His research focuses on hybrid photonic integrated circuits.

Madeleine Weigel received the master's degree in physics from the Technical University of Berlin, Berlin, Germany. She is currently working toward the Ph.D. degree with the Hybrid PICs Group, Fraunhofer Heinrich Hertz Institute (HHI), Berlin, working on 3-D photonic integration in polymer photonic integrated circuits. In 2017, she joined Fraunhofer Heinrich Hertz Institute (HHI), Berlin, as a Research Associate. She is currently the Project Manager with the Hybrid PICs Group, HHI.

Martin Kresse received the master's degree in physics from Berlin Technical University, Berlin, Germany. In 2018, he joined Fraunhofer Heinrich Hertz Institute (HHI), Berlin, as a Research Associate. He is currently working toward the Ph.D. degree from the Hybrid PICs Group on the topic of the hybrid photonic integration of tunable lasers.

Crispin Zawadzki received the diploma in electronic engineering from the Technical University of Berlin, Berlin, Germany, in 1995. In 1995, He joined Fraunhofer Heinrich Hertz Institute, Berlin. He is currently a Project Leader and has been responsible for process development and PLC/OEIC-fabrication in several research projects with national and international industrial partners. He holds several patents and has authored or coauthored more than 100 scientific publications and conference papers.

Björn Globisch studied physics in Aachen, and Berlin, Germany, and received the diploma degree in physics from the Technische Universität Berlin, Berlin, in 2011, and the Ph.D. degree in physics from the University of Marburg, Marburg, Germany, in 2017. He joined Fraunhofer Heinrich Hertz Institute (HHI), Berlin, as a Research Associate. Since 2017, he has been the Head of the Terahertz Sensor Systems Group, Fraunhofer HHI. Since 2019, he has also been an Associate Professor for terahertz sensing with the Institute Of Solid State Physics, Technische Universität Berlin. His research interests include transport and ultrafast phenomena in semiconductors, pulsed and continuous wave terahertz components and systems, and photonic integration.

Norbert Keil joined Fraunhofer Heinrich Hertz Institute, Berlin, Germany, in 1987. He has more than 30 years of experience in the development of polymer-based hybrid photonic integrated circuits. He is currently the Head of the Hybrid PICs Group and the Deputy Head of the Photonic Components Department. He holds several patents and has the authored or coauthored more than 200 scientific publications and conference papers.

Ronald Freund received the Dipl.-Ing. and Dr.-Ing. degrees in electrical engineering from the Technical University of Ilmenau, Ilmenau, Germany, in 1993 and 2002, respectively, and the MBA degree from RWTH Aachen University, Aachen, Germany. In 1997, he cofounded VPI Systems Inc., where he was a Chief Technology Officer and a Consultant, responsible for the development of design software for the physical layer of photonic networks. Since 1995, he has been with Fraunhofer Heinrich Hertz Institute, Berlin, Germany, where he is currently leading the Department of Photonic Networks and Systems. He has authored or coauthored more than 150 scientific publications. Since 2017, he has been appointed as a Professor for photonic communication systems with the Technical University of Berlin, Berlin.

Martin Schell received the Dipl.Phys. degree from RWTH Aachen University, Aachen, Germany, in 1989 and the Dr.rer.nat. degree from the Technical University of Berlin, Germany, in 1993. In 1995, he was Visiting Researcher at the University of Tokyo, Tokyo, Japan. From 1996 to 2000, he was Management Consultant at The Boston Consulting Group. From 2000 to 2005, he was Product Line Manager, and then Head of Production and Procurement, at Infineon Fiber Optics, Berlin. He is currently the Director of the Fraunhofer Heinrich Hertz Institute, Berlin and a Professor for optic and optoelectronic integration at the Technical University of Berlin. He is a Board Member of the European Photonics Industry Consortium, Chairman of the Competence Network Optical Technologies Berlin/Brandenburg (OptecBB), and Member of the Photonics21 Board of Stakeholders.